

This item is the archived peer-reviewed author-version of:

High-performance CO₂-selective hybrid membranes by exploiting MOF-breathing effects

Reference:

Kertik Aylin, Wee Lik H., Şentosun Kadir, Navarro Jorge A. R., Bals Sara, Martens Johan A., Vankelecom Ivo F. J..- High-performance CO₂-selective hybrid membranes by exploiting MOF-breathing effects
ACS applied materials and interfaces - ISSN 1944-8244 - 12:2(2020), p. 2952-2961
Full text (Publisher's DOI): <https://doi.org/10.1021/ACSAMI.9B17820>
To cite this reference: <https://hdl.handle.net/10067/1665760151162165141>

High-performance CO₂-selective Hybrid Membranes by Exploiting MOF-breathing Effects

Aylin Kertik, Lik Hong Hong Wee, Kadir Sentosun, Jorge A.R. Navarro, Sara Bals, Johan A. Martens, and Ivo F. J. Vankelecom

ACS Appl. Mater. Interfaces, **Just Accepted Manuscript** • DOI: 10.1021/acsami.9b17820 • Publication Date (Web): 20 Dec 2019

Downloaded from pubs.acs.org on December 22, 2019

Just Accepted

“Just Accepted” manuscripts have been peer-reviewed and accepted for publication. They are posted online prior to technical editing, formatting for publication and author proofing. The American Chemical Society provides “Just Accepted” as a service to the research community to expedite the dissemination of scientific material as soon as possible after acceptance. “Just Accepted” manuscripts appear in full in PDF format accompanied by an HTML abstract. “Just Accepted” manuscripts have been fully peer reviewed, but should not be considered the official version of record. They are citable by the Digital Object Identifier (DOI®). “Just Accepted” is an optional service offered to authors. Therefore, the “Just Accepted” Web site may not include all articles that will be published in the journal. After a manuscript is technically edited and formatted, it will be removed from the “Just Accepted” Web site and published as an ASAP article. Note that technical editing may introduce minor changes to the manuscript text and/or graphics which could affect content, and all legal disclaimers and ethical guidelines that apply to the journal pertain. ACS cannot be held responsible for errors or consequences arising from the use of information contained in these “Just Accepted” manuscripts.

High-performance CO₂-selective Hybrid Membranes by Exploiting MOF-breathing Effects

Aylin Kertik,[§] Lik H. Wee,^{§†*} Kadir Sentosun,[‡] Jorge A. R. Navarro,[‡] Sara Bals,[‡] Johan A. Martens,[§] Ivo F. J. Vankelecom^{§*}

[§]Center for Surface Chemistry and Catalysis, University of Leuven, Celestijnenlaan 200F, Post Box- 2461, B3001, Leuven, Belgium.

[‡]Electron Microscopy for Materials Science, University of Antwerp, Groenenborgerlaan 171, B2020, Antwerp, Belgium.

[‡]Departamento de Química Inorgánica, Universidad de Granada, Av. Fuentenueva S/N, 18071 Granada, Spain.

KEYWORDS: metal-organic framework; breathing; crosslinking; mixed-matrix membranes; gas separation

ABSTRACT

Conventional CO₂ separation in the petrochemical industry via cryogenic distillation or amine-based absorber-stripper units is energy intensive and environmentally unfriendly. Membrane-based gas separation technology, on the other hand, has contributed significantly to the development of energy-efficient systems for e.g. natural gas purification. The implementation of commercial polymeric membranes in gas separation processes is restricted by their permeability-selectivity trade-off and by their insufficient thermal and chemical stability. Herein, we present the fabrication of Matrimid[®]-based membrane loaded with a breathing metal-organic framework

(MOF) (NH₂-MIL-53(Al)) which is capable of separating binary CO₂/CH₄ gas mixtures with high selectivities without sacrificing much of its CO₂ permeabilities. NH₂-MIL-53(Al) crystals were embedded in a polyimide (PI) matrix and the mixed-matrix membranes (MMMs) were treated at elevated temperatures (up to 350 °C) in air to trigger PI crosslinking and to create PI-MOF bonds at the interface to effectively seal the grain boundary. Most importantly, the MOF transitions from its narrow-pore form to the large-pore form during this treatment, allows the PI chains to partly penetrate the pores and crosslink with the amino functions at the pore mouth of the NH₂-MIL-53(Al) and stabilizes the open-pore form of NH₂-MIL-53(Al). This crosslinked MMM, with MOF pore entrances made more selective by the anchored PI-chains, achieves outstanding CO₂/CH₄ selectivities. This approach provides significant advancement towards the design of selective MMMs with enhanced thermal and chemical stabilities which could also be applicable for other potential applications, such as separation of hydrocarbons (olefin/paraffin or isomers), pervaporation and solvent resistant nanofiltration.

Introduction

Purification of natural gas, also known as natural gas sweetening, is the largest industrial separation involving removal of CO₂ from CH₄.¹⁻³ Many natural gas wells contain significant amounts of CO₂, which have to be removed prior to delivery to pipelines to minimise corrosion and to increase calorific value.¹ Raw biogas generated from biomass and organic wastes contains primarily of 55-65% of methane and 35-45% of CO₂. Biogas upgrading to achieve biomethane with concentration above 90% similar to the natural gas standard is of economic importance. Both types of gas upgrading can very well be performed with membrane technology.

1
2
3 Among the membranes developed for gas treatment, only polymeric membranes have been
4 commercialized so far.^{6,7} An important search is still ongoing for membranes with higher
5 selectivity without permeance loss, together with enhanced thermal and chemical stability.⁷
6
7 Currently, the typical CO₂/CH₄ selectivity in industrial separations is limited due to the
8 permeability-selectivity trade-off for polymeric membranes, as reflected in the Robeson upper-
9 bound.^{1,8,9} Another major challenge of polymer membranes for gas separation is related to their
10 susceptibility to plasticization at high CO₂ partial pressures when polymer membranes encounter
11 an undesirable loss in separation power. CO₂ then excessively swells the polymer and eases the
12 permeation of CH₄, thus reducing selectivities.⁶ Membrane crosslinking is one of the best ways to
13 handle this plasticization.¹⁰⁻¹²
14
15
16
17
18
19
20
21
22
23
24
25
26

27 Mixed-matrix membranes (MMMs) composing of homogeneously dispersed fillers in a
28 polymeric matrix aim to combine the advantageous of polymer processibility and the superior
29 separation properties of the porous fillers.¹³⁻¹⁹ Metal-organic frameworks (MOFs) have attracted
30 considerable attention owing to their tailorable functionality, tunable pore size and breathing
31 effects.^{20,21} Breathing of MOFs refers to a structural transition, involving the reversible opening or
32 contraction of pores.^{22,23} MIL-53 is one of the best representatives of such “breathing” MOFs.²⁴ It
33 is constructed from MO₄(OH)₂ octahedra (M= Fe³⁺, Cr³⁺, Al³⁺ or Ga³⁺) and terephthalate (BDC)
34 linkers, exhibiting the unique transition of large-pore (*lp*, 8.5 Å x 8.5 Å) to narrow-pore (*np*, 2.6
35 Å x 13.6 Å) form by inducing a unit cell volume change upon the inclusion of guest molecules
36 (e.g. water, CO₂ and xylene) or external stimuli (e.g. pressure and heat).²⁴⁻²⁸ As-synthesized MIL-
37 53 consists of trapped unreacted BDC molecules in the pores and gives the *lp* configuration. These
38 BDC species can be evacuated upon heating at 320 °C, resulting in an open-pore framework. The
39 open-pore framework will absorb water molecules upon cooling to room temperature to give the
40
41
42
43
44
45
46
47
48
49
50
51
52
53
54
55
56
57
58
59
60

1
2
3 *np* configuration. The absorbed water molecules interact with the hydroxyl groups of the inorganic
4 cluster through strong H-bonding. The breathing MIL-53(Al) is known for its unusually high
5 adsorptive selectivity for CO₂ over CH₄ via the quadrupolar interaction of CO₂ with the corner-
6 sharing hydroxyl groups of the MIL-53 pore wall.²⁹ A similar topology but with amine-
7 functionalization could be synthesized by replacing the terephthalic acid with 2-
8 aminoterephthalic acid.³⁰⁻³² NH₂-MIL-53(Al) has diamond shaped channels with a pore diameter
9 of 7.5 x 7.5 Å and with amino groups that point inwards to the pore.³² Unlike many amino-
10 functionalized materials, NH₂-MIL-53(Al) does not form a chemical bond between CO₂ molecules
11 and the NH₂ groups. Instead, the amino functions regulate the breathing behaviour, resulting in
12 superior separation factor for CO₂ over CH₄.²⁵ The interaction of the decorated amino functions
13 with the aluminium-occupied oxygen octahedra in the framework structure stabilizes the NH₂-
14 MIL-53(Al) *np* form via hydrogen bonding. As a result, the energy losses associated with the
15 structural perturbations upon formation of the *np* structure is reduced, and thus contributing
16 towards the enhanced local flexibility of the inorganic trans-corner-sharing [AlO₆] chains. This
17 synergistic effect leads to NH₂-MIL-53(Al) structure with greater structural stability in its *np* form.
18 The stable *np* starting form allows it to effectively pack CO₂ molecules while exclusively hindering
19 the adsorption of other molecules with larger kinetic diameter such as CH₄. Moreover, the presence
20 of structural amino and hydroxyl functional groups in MIL-53 also play an important role to
21 enhance the host-guest interaction with CO₂, contributing to a high CO₂/CH₄ selectivity.²⁵
22
23
24
25
26
27
28
29
30
31
32
33
34
35
36
37
38
39
40
41
42
43
44
45
46
47

48 Excellent selectivities have been recently reported using CuBDC nanosheets³³ or ZIF-8³⁴
49 as MOF fillers in MMMs for CO₂/CH₄ separations. NH₂-MIL-53 as a powder possessed high
50 selectivity in CO₂/CH₄ separation, but failed to reach the 2008 Robeson upper bound for CO₂/CH₄
51 in MMM separations, especially due to low selectivities. Probably, this is mainly due to polymer-
52
53
54
55
56
57
58
59
60

1
2
3 MOF interstitial defects and the too open pore configuration of the MOF in the membranes. The
4
5 results highlight the challenge to regulate the MOF breathing behaviour to enable their use in
6
7 selective membrane gas separations.^{35,36} Recently, we reported an in-situ thermally induced
8
9 amorphization of ZIF-8 in a PI matrix. The thermal treatment simultaneously enhances MOF-PI
10
11 interactions via oxidative crosslinking to effectively seal the interfacial voids/grain boundaries.
12
13 This new hybrid crosslinked membrane showed enhanced chemical and thermal stabilities,
14
15 together with very high CO₂/CH₄ mixed gas selectivities.³⁷ In present work, the remarkable
16
17 breathing effect of NH₂-MIL-53(Al) MOF is exploited by maintaining the *lp* structure, regardless
18
19 guest molecule, pressure or temperature, via controlled thermal treatment of the MOF at 350 °C
20
21 while embedded in the polymer matrix. During this treatment, the PI membrane matrix is
22
23 crosslinked. Simultaneously, the polymer chains are penetrated into the *lp* pores, where they link
24
25 covalently to the amino functions decorated on the pore walls of NH₂-MIL-53(Al). Upon cooling,
26
27 the MOF retains the *lp* form, while the region around the pore mouth gets densified and became
28
29 more selective. The *lp* structure of NH₂-MIL-53(Al) anchored with polymer chains at the pore
30
31 mouth shows remarkable selectivity in CO₂/CH₄ separation, while retaining the membrane
32
33 permeabilities.
34
35
36
37
38
39
40

41 **Experimental Methods**

42 **Materials**

43
44
45 Commercially available polyimide (PI, Matrimid 5218) was kindly provided by Huntsman and
46
47 used after drying at 110 °C overnight. For NH₂-MIL-53(Al) synthesis, the linker source 2-
48
49 aminoterephthalic acid (NH₂BDC, H₂NC₆H₃-1,4-(CO₂H)₂, 99+%) and the Al source aluminum
50
51 nitrate nonahydrate (Al(NO₃)₃·9H₂O, 98.5+%) were obtained from ChemLab and Acros Organics,
52
53
54
55
56
57
58
59
60

1
2
3 respectively, and used without further treatment. The solvents used in the solvent exchange and
4
5 membrane preparation were dimethylformamide (99+%), chloroform (99.8%), and methanol
6
7 (99.8%), purchased from Acros Organics.
8
9

10 11 **Synthesis of NH₂-MIL-53(Al)**

12
13
14 The synthesis of NH₂-MIL-53(Al) was achieved by dissolving NH₂BDC (2 g) and Al(NO₃)₃·9H₂O
15
16 (2 g) in distilled water (400 mL). The solution was stirred at 100 °C for 6 hours. Upon cooling, the
17
18 MOF particles were separated by centrifugation and washed using DMF, methanol and
19
20 chloroform, respectively. Following the final centrifugation step, the remaining MOF sludge was
21
22 re-distributed in CHCl₃ and stored in wet form. The synthesis of NH₂-MIL-53(Al) nanoparticles
23
24 was carried out by dissolving Al(NO₃)₃·9H₂O (0.7602 g) in 7.50 ml of distilled water and NH₂BDC
25
26 (0.5601 g) in 22.50 ml of DMF.⁴⁹ After mixing the two solutions and stirring for 1 h, the final
27
28 solution was transferred into a 100 ml stainless steel autoclave, followed by inducing reaction at
29
30 150 °C for 24 h. Upon cooling, the synthesized MOF particles were separated by centrifugation
31
32 and washed with DMF, methanol and chloroform, respectively. After the final centrifugation step,
33
34 the collected MOF sludge was re-distributed in CHCl₃ and stored in wet form.
35
36
37
38
39

40 41 **Fabrication of PI-NH₂-MIL-53(Al) MMMs**

42
43
44 MMMs with 20, 30 and 40 wt% MOF loadings were fabricated. MOF mixture was weighed to
45
46 provide the MOF content to achieve the desired MOF loading and the Matrimid[®] that was dried
47
48 overnight at 110 °C was added and dissolved to this mixture. A polymer concentration of 7 wt%
49
50 was kept to achieve a moderately viscous solution that still allows membrane casting, but would
51
52 prevent MOF precipitation upon casting. The membrane mixture was stirred until the polymer was
53
54 fully dissolved. Proving the effectiveness of membrane preparation starting from a MOF sludge,
55
56
57
58
59
60

1
2
3 extra mixing step with e.g. ultrasonication was not needed in order to achieve excellent MOF
4 particle distribution. The MOF loading of membranes was calculated as given in the following
5 equation:
6
7
8
9

$$10 \text{ Loading (wt. \%)} = 100 * \frac{wt_{\text{MOF}}}{wt_{\text{MOF}} + wt_{\text{polymer}}}$$

11
12
13 where, wt_{MOF} and wt_{polymer} are amount of MOF and polymer, respectively. Petri dishes specifically
14 designed for membrane casting were used to ensure uniform membrane thickness. The petri dishes
15 consist of glass rings attached to flat glass surfaces. Upon casting, the membrane solution was left
16 to dry overnight at room temperature in inert N_2 atmosphere. The inert N_2 atmosphere prevented
17 contact with the humidity in air. The vitrified membranes were peeled off carefully from the petri
18 dish and annealed in ovens. Glass supports were used to sandwich membranes and to prevent
19 curving. The oven was gradually heated, starting from room temperature to 100 °C (above the
20 boiling point of CHCl_3), 160 °C (slightly exceeding the boiling point of DMF), 250 °C (between
21 the boiling point of DMF, and the Tg of Matrimid®) or 350 °C (above the Tg of Matrimid®). Each
22 heating step was designed to increase the temperature by 1°C/min with 50 °C increments. The
23 oven remained isothermal for 2 hours at each increment. The membranes were kept at the final
24 temperature for 24 hours, and subsequently removed after the oven was allowed to cool down to
25 room temperature naturally. Immediate quenching was avoided as it is known to cause void
26 formation between the polymer and the filler as a result of the differences in the thermal expansion
27 coefficients. The polymer-MOF attachment was preserved by allowing the MMMs to cool down
28 naturally.
29
30
31
32
33
34
35
36
37
38
39
40
41
42
43
44
45
46
47
48
49

50 **Characterization of MMMs**

51
52
53 Attenuated total reflectance Fourier transform infrared spectroscopy (ATR-FTIR) was carried out
54 in air using a Varian 620 FT-IR imaging microscope with a Germanium crystal. FTIR spectra were
55
56
57
58
59
60

1
2
3 collected over a wavelength range from 400 to 4000 cm^{-1} with a spectral resolution of 4 cm^{-1} and
4
5 64 scans. Cross-sectional SEM imaging of the membrane was taken using a JEOL JSM-1060LV
6
7 scanning electron microscope (SEM). If a membrane was sufficiently flexible, it was freeze-
8
9 fractured. The membranes that were already too brittle were broken in liquid N_2 . The samples were
10
11 sputtered with Au/Pd for three cycles of 20 seconds in order to prevent charge build-up. Charge
12
13 build-up during SEM analysis happens as a result of the non-conductive nature of the polymers,
14
15 X-ray diffraction (XRD) patterns were obtained by using a Stoe-HT X-ray diffractometer, with
16
17 $\text{CuK}\alpha$ radiation, $\lambda=1.54 \text{ \AA}$ at room temperature. The mechanical strength of the membrane samples
18
19 were tested at room temperature using a Universal Testsystem (UTS) with 0.0001 mm position
20
21 resolution and load cells up to 200 N. A TA Instruments DSC Q2000 using Al hermetic closed
22
23 pans and in N_2 atmosphere was used for differential scanning calorimetry (DSC) measurements.
24
25 The samples were first stabilised at 20 $^\circ\text{C}$ for 10 minutes, then heated to 370 $^\circ\text{C}$ at 10 $^\circ\text{C}/\text{minute}$.
26
27 After 5 minutes, the samples were cooled to 20 $^\circ\text{C}$ at 10 $^\circ\text{C}/\text{minute}$ and re-heated to 370 $^\circ\text{C}$ as
28
29 described. The thermogravimetric behaviour of samples was analysed with TA Instruments TGA-
30
31 Q500. The temperature was increased from room temperature to 100 $^\circ\text{C}$ at 5 $^\circ\text{C}/\text{min}$, maintained
32
33 at this temperature for 10 minutes, then heated to 160 $^\circ\text{C}$ at 2 $^\circ\text{C}/\text{min}$, maintained at this
34
35 temperature for 10 minutes, and finally to 500 $^\circ\text{C}$ at 10 $^\circ\text{C}/\text{min}$. The ambient atmosphere (N_2 or
36
37 O_2) is appropriately reported in the results section. The membrane samples were prepared for TEM
38
39 by gluing the sample on a support to fit the holder of the microtome. It was not necessary to embed
40
41 the samples in epoxy resin, as the samples consisted of polymeric membrane, The samples were
42
43 then sliced with a 100 nm thickness using a Leica UC7 ultramicrotome equipped with a histo
44
45 diamond knife. Selected area electron diffraction (SAED) patterns, high resolution TEM
46
47 (HRTEM) and high angle annular dark field scanning TEM (HAADF-STEM) images were
48
49
50
51
52
53
54
55
56
57
58
59
60

1
2
3 acquired using a FEI Osiris microscope, operated at 200 kV. Energy dispersive X-ray spectroscopy
4
5 (EDX) maps were acquired using a ChemiSTEM system, the data was analysed using the Bruker
6
7 ESPRIT software.
8
9

10 11 **Gas Separation** 12 13

14 The membranes were tested for gas separation performance using binary gas mixtures. The gas
15
16 separation system is a custom-built, high-throughput gas separation system (HTGS), described in
17
18 detail in ref. 32. The membranes were tested at 35 °C and 10 bar cross-membrane pressure
19
20 difference using a CO₂/CH₄ mixture of 50-50% vol. composition. The gas composition at the
21
22 permeate side was determined using gas chromatography (GC). The membranes were first flushed
23
24 with the gas mixture overnight to reach steady-state. Steady-state was confirmed by comparing
25
26 consecutive GC measurements to yield the same result. Once steady-state was confirmed, three
27
28 more measurements were carried out on the gas accumulated on the permeate side. The average of
29
30 these three measurements was reported as a data point. Every data point was obtained from
31
32 averaging the data collected from two membranes prepared from the same batch and two coupons
33
34 from each membrane. The reported data for every coupon was calculated as an average of three
35
36 measurements for both permeability and selectivity after steady state was reached. The MMM
37
38 coupon has a surface area of 2.24 cm² and the active permeation area is 1.54 cm². The
39
40 permeabilities were measured at steady-state using a constant-volume variable-pressure
41
42 permeation system. The overall permeability (P_o) and the relative permeability of CO₂ (P_{CO₂}) were
43
44 calculated using equations as follows, respectively.³⁸
45
46
47
48
49
50

$$51$$
$$52$$
$$53 P_o = \frac{\alpha V l}{A R T \Delta P}$$
$$54$$
$$55$$
$$56$$
$$57$$
$$58$$
$$59$$
$$60$$

1
2
3 where, α represents the pressure increase rate in the permeate side with respect to time, V is the
4 volume of the permeate side, l is the membrane thickness, A is the membrane surface area, R is
5 the ideal gas constant, T is the permeation temperature, and ΔP is the cross-membrane pressure
6 difference.
7
8
9

$$P_{\text{CO}_2} = P_o \frac{y_{\text{CO}_2}}{x_{\text{CO}_2}}$$

10
11
12
13
14
15
16 where, P_o refers to the overall permeability, y_{CO_2} and x_{CO_2} denote the CO_2 content at the permeate
17 and feed sides, respectively.³⁸
18
19
20
21

22 **Results and Discussion**

23
24
25
26
27
28
29
30
31
32
33
34
35
36
37
38
39
40
41
42
43
44
45
46
47
48
49
50
51
52
53
54
55
56
57
58
59
60

MMMs with various $\text{NH}_2\text{-MIL-53(Al)}$ loadings (20, 30 and 40 wt%) were prepared. The as-synthesized $\text{NH}_2\text{-MIL-53(Al)}$ filler has a particle size ranges between 300 to 600 nm according to SEM imaging (Figure S1). MMMs with different $\text{NH}_2\text{-MIL-53(Al)}$ loadings (20-40 wt%) were prepared and thermally treated at 100, 160, 250 or 350 °C in air for periods up to 24h. The well-controlled thermal treatment at 350 °C in air induced a significant change in membrane colour, as shown in Figure 1A. The PI membrane turned from yellow to dark-brown at 350 °C, whereas the MMMs started to darken at lower temperatures already. The changes of color of the membranes from yellow to dark brown upon heat treatment at 350 °C maybe due to physicochemical changes (e.g. formation of charge transfer complexes) in the membrane during the heating. Similar observation has also been noted for other polymer membranes such as PIM-1³⁹ and poly(ether-block-amide) copolymer⁴⁰ membranes upon heat treatment. According to TGA (Figures 1B and S2), bulk $\text{NH}_2\text{-MIL-53(Al)}$ starts to decompose at 200 °C. The presence of the surrounding PI-matrix significantly improved the thermal stability of the $\text{NH}_2\text{-MIL-53(Al)}$ up to >400 °C, in line with other systems.³⁷ A significant weight loss before 120 °C as noted for the MMMs treated at

250 and 350 °C is due to the water formation as a result of the chain termination reaction.⁴¹ Solubility tests after 2 days of immersion in chloroform (Figure S3) showed that the membranes treated at 160 °C were completely soluble, whereas the MMMs treated at higher temperatures had become insoluble in chloroform, showing a high gel content above 90% after 2 days (Figure S3), confirming the enhanced chemical stability.

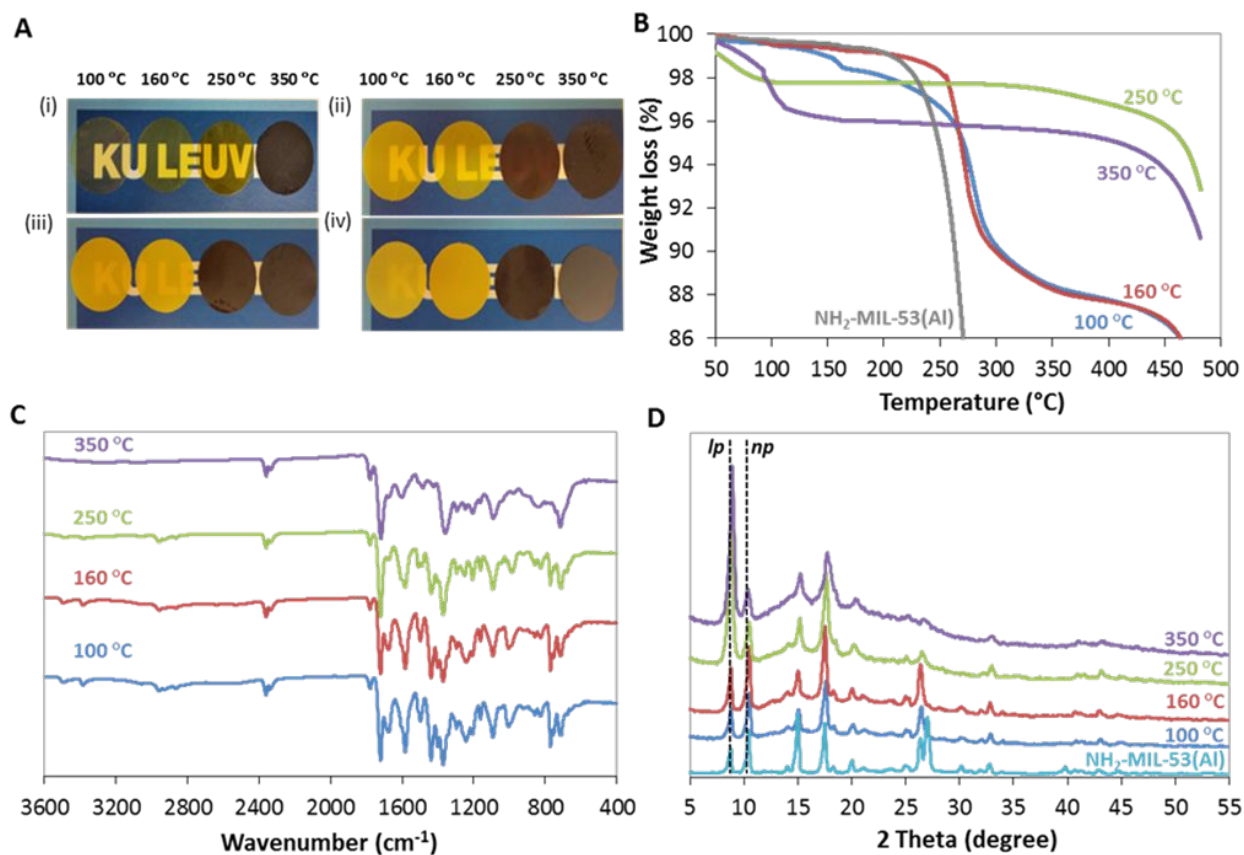
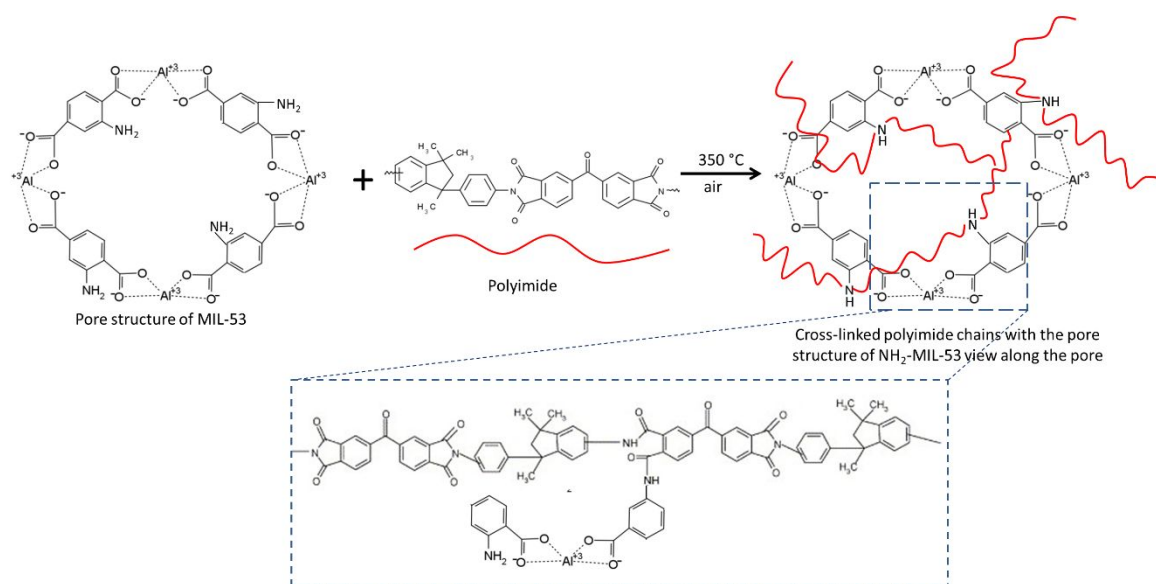


Figure 1. Solubility, Thermal, Chemical and Structural Properties of Thermally Treated MMMs.

A) The change in colour of the (i) unfilled Matrimid® membranes and MMMs with different MOF loading (ii) 20 wt%, (iii) 30 wt% and (iv) 40 wt% with increasing treatment temperature. B) TGA profiles, C) FTIR spectra and D) XRD patterns of MMMs with 40 wt% NH₂-MIL-53(Al) loading treated at different temperatures in comparison to bulk NH₂-MIL-53(Al). Enlarged versions of

1
2
3 ATR-FTIR spectra marked with characteristic peaks assigned to thermo-oxidative crosslinking of
4 Matrimid® and MMMs treated at different temperatures are provided in Figure S4.
5
6
7

8
9 The improved thermal and chemical stabilities of the MMMs confirmed the expected oxidative PI-
10 crosslinking.³⁷ In order to confirm this phenomenon and to provide insight into the interactions
11 between the polymer and the embedded MOF, the MMMs were characterized by ATR-FTIR
12 (Figures 1C and S4). Oxidative crosslinking of Matrimid® occurs through the C-H groups is
13 confirmed according to the observed reduction in intensity of the characteristic bands
14 corresponding to the aliphatic C-H stretching (2954, 2921 and 2860 cm^{-1}) (Figure S4). The
15 thermally-induced oxidative crosslinking of the polymer due to the combination of radical sites on
16 adjacent chains has been previously described in detail.³⁷
17
18
19
20
21
22
23
24
25
26
27



47 **Scheme 1.** Schematic showing the mechanism of chemical crosslinking of polyimide polymer
48 chains with the amino functions at the pore entrance of NH₂-MIL-53(Al) upon thermal treatment
49 at 350 °C in air.
50
51
52
53
54
55
56
57
58
59
60

1
2
3 The bands at 1774 and 1716 cm^{-1} are assigned to the symmetric and asymmetric stretching
4 of the C=O groups of the polymer imide (Figure S4).⁴² The 1365 cm^{-1} absorption band is attributed
5 to the C–N stretching of the imide five-membered ring of the polyimide membrane. The
6 crosslinking of amino functions (NH_2 -MIL-53) with the polymer chains at the pore mouth is
7 confirmed via the appearance of the amide signals at 1538 cm^{-1} which is attributed to N–H bending
8 and the disappearance of the two bands at 3352 and 3482 cm^{-1} related to the symmetric and
9 asymmetric vibrations of NH_2 groups of NH_2 -MIL-53(AI), respectively.^{42,43} Also, the transverse
10 stretching of C–N–C at 1084 cm^{-1} which characterizes the presence of the imide groups were also
11 found to decrease. However, the intensity of these absorption bands are not significant mainly due
12 to the relatively low concentration of formed amide groups between the MOF particles and
13 polymer matrix at the interface as only the terminal amino functions at the outer surface of the
14 MOFs will take part for this specific crosslinking reaction. Similar observations of polyimide-
15 MOF interaction has also been reported.^{42,43} The crosslinking process is initiated by the attack of
16 the imide functional groups of Matrimid[®] at the amino groups of the bridging terephthalates,⁴⁴
17 most probably occurs at the pore mouth. (Scheme 1). The PI-bulk crosslinking and the reduced
18 chain mobility at the MOF-polymer interface were directly reflected in the T_g of the membranes,⁴⁵
19 where an increase in the T_g values from 318 to 326, 328 and 337 $^\circ\text{C}$ were noted with 20, 30 and
20 40 wt% loading, respectively. Similarly, the tensile strength of the membranes was also induced
21 as the crosslinking temperature increases, as shown in the Table S1 and Figure S5.
22
23
24
25
26
27
28
29
30
31
32
33
34
35
36
37
38
39
40
41
42
43
44
45
46
47

48 XRD patterns of the MMMs (Figures 1D and S6-S9) reveal that the structure of MIL-53
49 was preserved, despite a sign of crystallinity loss, after treatment at 350 $^\circ\text{C}$. It was noted from the
50 TG analyses that the MMMs treated at high temperatures (250 and 350 $^\circ\text{C}$) exhibit an enhanced
51 thermal stability up to 400 $^\circ\text{C}$, whereas the MMMs annealed at lower temperatures (160 and 100
52
53
54
55
56
57
58
59
60

1
2
3 °C) start to decompose at 200 °C. Similar thermal behaviour was observed for bulk NH₂-MIL-
4 53(Al). The results suggest that the thermal cross-linking significantly enhanced the thermal
5 stability of the NH₂-MIL-53(Al) embedded in the polymer matrix. NH₂-MIL-53(Al) is a flexible
6 MOF.^{25,46,47} The removal of the trapped molecules triggers the direct structural change from either
7 the *np* form (*np* guest such as H₂O) or the *lp* form (*lp* guest such as DMF and terephthalic acid) to
8 the empty *lp* form upon activation above 100 °C. This material transforms to the *np* phase after
9 cooling under ambient conditions due to adsorption of water molecules. Adsorption of CO₂ could
10 also induce the transition from the *lp* to the *np* form. However, for the case of NH₂-MIL-53(Al) in
11 its hydrated form, CO₂ adsorption at low pressures only produces minor structural changes due to
12 stronger hydrogen-bonds interaction in the framework structure.^{25,47} Only at higher partial pressure
13 above 10 bar, the *np* form will expand to its *lp* form.⁴⁷ This observation was further confirmed by
14 XRD (Figure 1D), showing exclusively the *np* configuration for bulk NH₂-MIL-53(Al) and the
15 MMMs treated at low temperature (100 and 160 °C). Interestingly, the embedded NH₂-MIL-
16 53(Al) in the polymer matrix showed the *lp* form after heating the MMM above 160 °C.⁴⁸⁻⁵⁰
17 Although such transition normally occurs in presence of penetrants, such as DMF⁵⁰ or CO₂,⁵¹ in
18 the MOF pores, the FTIR (Figures 1C and S4) and TGA results (Figures 1B and S2) however,
19 confirm the absence of any adsorbed species. The lack of FTIR signals in the 1673–1690 cm⁻¹
20 range, assigned to the amide group of the DMF, indeed indicates that the MOF was well-washed
21 and solvent exchanged with methanol and chloroform. Moreover, the TGA curves do not exhibit
22 any observable weight loss around the boiling point of DMF (153 °C). The *np* form of NH₂-MIL-
23 53(Al) is energetically preferred over the *lp* form. Hence, the *np* form should prevail again after
24 cooling down. The expanded MOF framework in the MMMs is however retained, as evidenced by
25 the XRD patterns. Such observation can be ascribed to the (at least partial) penetration and
26
27
28
29
30
31
32
33
34
35
36
37
38
39
40
41
42
43
44
45
46
47
48
49
50
51
52
53
54
55
56
57
58
59
60

1
2
3 chemical fixation of the PI chains in the NH₂-MIL-53(Al) pores. As proven above, covalent
4 bonding between the polymer and the amino functions on the pore walls takes place at these high
5 temperatures, thus leaving no possibility for the MOF-structure to relax again upon cooling.
6
7 Penetration of polymer chains into the *lp* pore can be characterized by the glass transition
8 temperature (T_g).⁵² For the 40 wt% NH₂-MIL-53(Al) loaded MMM treated at 100 °C, in which
9 the NH₂-MIL-53(Al) has the *np* form, the measured T_g was 318 °C. For the 40 wt% NH₂-MIL-
10 53(Al) loaded MMM treated at 350 °C, in which the NH₂-MIL-53(Al) has an *lp* form, the measured
11 T_g was 337 °C. A significant 19 °C increase in T_g temperature is indicative for polymer
12 penetration into the open pore structure of NH₂-MIL-53(Al). A similar observation has also been
13 reported for the penetration of polymer chains into the open pore structure of MIL-53⁵² and
14 mesoporous ZSM-5⁵³ loaded Matrimid membranes. Direct evidence of polymer chain penetration
15 into the pore structure of UiO-66 embedded in the polymer matrix has also been confirmed by
16 solid-state NMR studies⁵⁴ and molecular simulations.⁵⁵

17
18
19
20
21
22
23
24
25
26
27
28
29
30
31
32
33
34 Figure S10 shows the cross-sectional SEM images of unfilled PI membranes and MMMs
35 with 20, 30 and 40 wt% loading. The unfilled PI membranes do not show observable change in
36 morphology with increasing treatment temperature. For MMMs, the NH₂-MIL-53(Al) (light
37 regions) and polymer (dark regions) can be clearly identified by the contrast between the two
38 nanostructure phases. With the present MIL-53-Matrimid[®] system, the polymer and the MOF
39 create a perfectly homogeneous MMM even at high MOF loading. When the MMMs were
40 thermally treated at 350 °C, thus surpassing the T_g of Matrimid[®] (~305 °C) under controlled heating
41 and cooling, the polymer chains are expected to adhere much better to the surface of the MOF
42 particles, considering the chemical nature of the MOF linker which shows many possibilities for
43 physico-chemical interactions with the PI chain (e.g. π -stacking and H-bonding).^{56,57}

1
2
3 Interfacial voids at grain boundaries in MMMs are detrimental to membrane selectivity.
4
5 They are created by poor polymer-filler interactions and are frequently encountered in MMMs,
6
7 especially at high loadings.⁵⁸ A combination of high angle annular dark field scanning transmission
8
9 electron microscopy (HAADF-STEM), selected area electron diffraction (SAED) and energy
10
11 dispersive X-ray (EDX) analysis was performed in order to provide insight into the
12
13
14
15
16
17

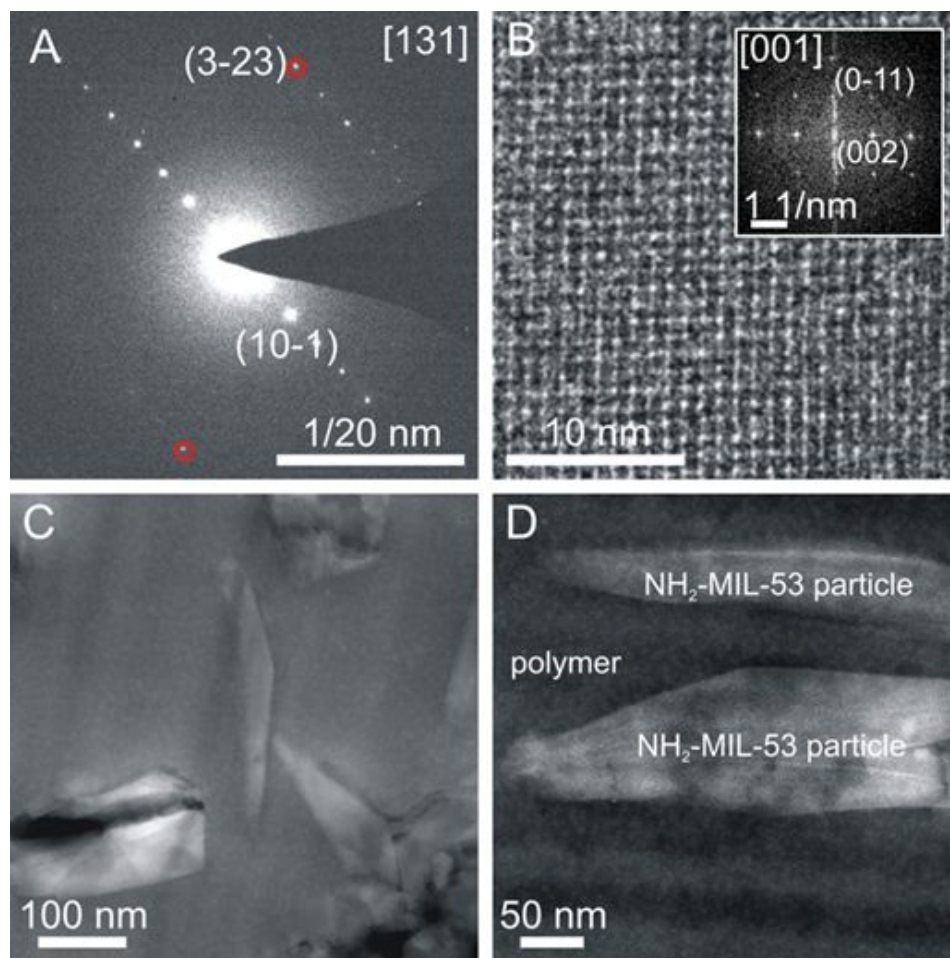


Figure 2. Advanced TEM characterization of MMM with 40 wt% NH₂-MIL-53(Al) Loading. A) SAED pattern recorded along [131] zone axis from NH₂-MIL-53(Al) nanoparticle. B) HRTEM

1
2
3 micrograph and corresponding FFT pattern from a similar particle as in (A). C and D) HAADF-
4
5 STEM image displaying the morphology of NH₂-MIL-53(Al) particles embedded in a MMM.
6
7
8
9

10
11 compatibility of the MOF with the PI as well as the crystallinity of the embedded NH₂-MIL-53(Al).
12
13 The results confirm that the crystallinity of the incorporated NH₂-MIL-53(Al) is preserved (Fig.
14
15 2A). Since the structure and morphology of the fillers change quickly under electron beam
16
17 irradiation, a low dose electron beam was selected to record reliable diffraction data. Figure 2B
18
19 displays an HRTEM micrograph acquired from a similar particle along the [001] zone axis. The
20
21 measured *d*-values and diffraction angles from the SAED pattern are in strong agreement with the
22
23 known orthorhombic *lp* form structure model (space group: *Imma*), in full agreement with the
24
25 XRD results (Figure 1D) and as reported elsewhere.⁵⁹ An overview of HAADF-STEM images
26
27 depicting the morphology of the particles embedded inside the MMM is presented in Fig. 2C and
28
29 2D. The TEM images (Figures 2C and 2D) reveal excellent compatibility at the filler-PI interface.
30
31 The blue arrows indicate a dark contrast at the interface between the particles and the MMM,
32
33 mainly due to cutting artefacts during the sample preparation. The chemical distribution of the
34
35 individual Al and O elements visualized by EDX mapping (Figures S10B and S10C) was acquired
36
37 from the red highlighted region in Figure S11A, confirming the presence of incorporated NH₂-
38
39 MIL-53(Al) in the polymer matrix.
40
41
42
43
44
45
46

47
48 Figure 3 and Table S2 show the mixed-gas permselectivity as a function of the heat
49
50 treatment temperature for unfilled Matrimid® and MMMs with different loadings. The CO₂/CH₄
51
52 selectivity increases with increasing filler loadings. Especially at the maximal loading (40 wt%),
53
54 a high CO₂/CH₄ selectivity of 153 was achieved without sacrificing much CO₂ permeability. To
55
56
57
58
59
60

investigate the accessibility of the MMM by the permeating gas, single CO₂ adsorption isotherms were measured of the MMMs with 40 wt% MOF loading treated at different temperatures (Figure S12). The isotherms revealed that the composite membranes are accessible to CO₂. However, it should be noted that the accessibility of MMMs to CO₂ adsorption is reduced particularly upon

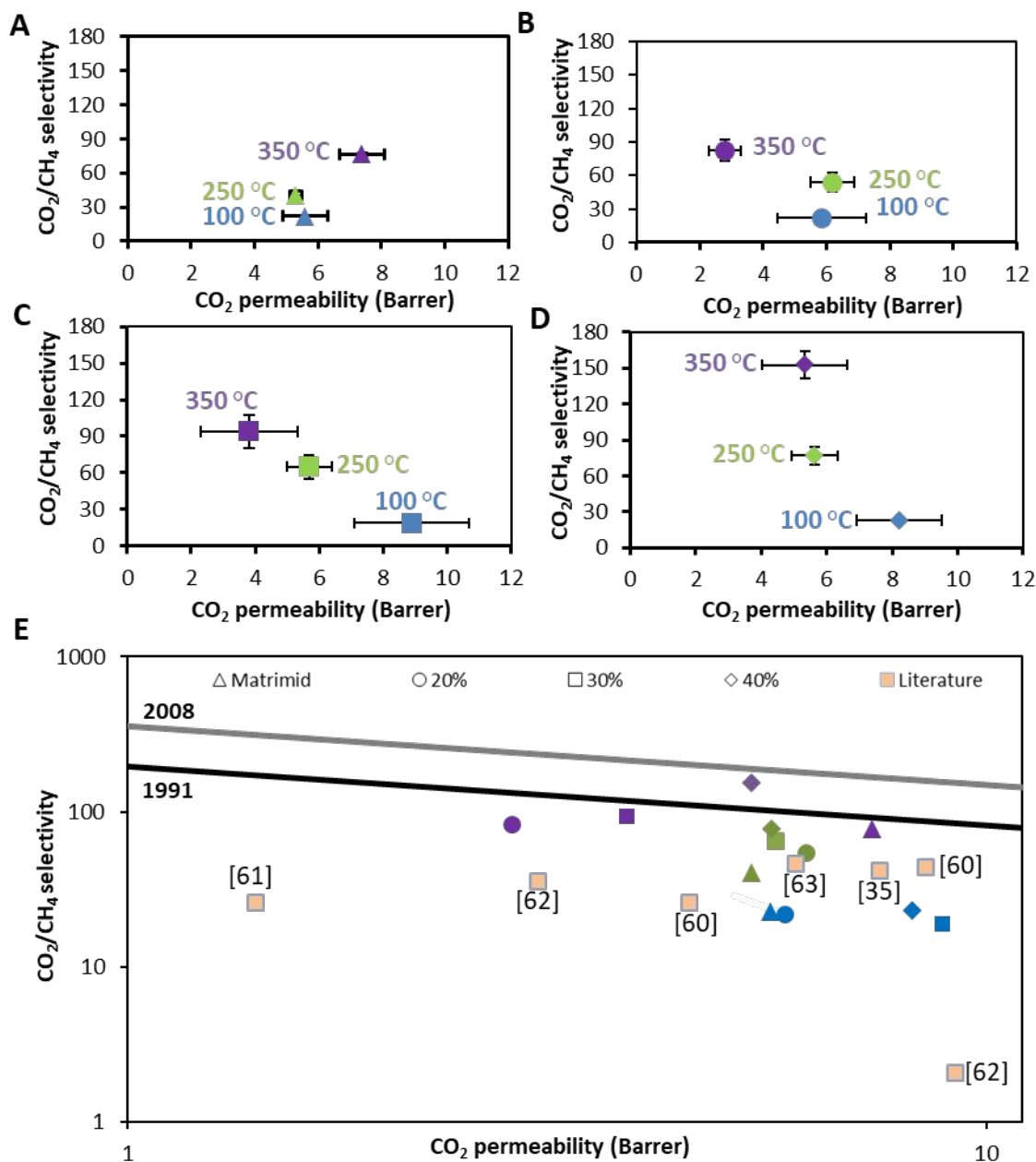


Figure 3. The Evolution of the separation performance of the thermally treated membranes. A)

1
2
3 Matrimid[®] and B-D) MMMs with 20, 30 and 40 wt% NH₂-MIL-53(Al) loading treated at
4 increasing annealing temperature. E) The Robeson plot of 1991 and 2008 compared with the
5 results from literature (orange squares), and results obtained from this work (blue: 100 °C; green:
6 250 °C and purple: 350 °C). A detailed comparison of all MOF loaded MMMs results with all
7 MOF-loaded MMM together with the measurement conditions is presented in Table S2.
8
9
10
11
12
13
14
15
16
17
18

19 thermal treatment at 350 °C mainly due to densification of the composite membranes as a result
20 of polymer-polymer and polymer-filler crosslinking, in full agreement with the gas separation
21 results. It should be mentioned that the unfilled Matrimid[®] membranes treated at 100 °C only show
22 a CO₂/CH₄ selectivity of 22 under similar conditions (Table S2). The results suggest that a
23 relatively high filler loading is required in order to maximally gain from the effect of incorporating
24 MOF crystals in the PI matrix. In most other cases,⁶⁴ selectivities start to drop significantly at these
25 higher loading due to creation of defects, proving again the excellent MOF-PI interactions realized
26 here. In order to study whether the enhanced selectivity achieved from the crosslinked MMMs was
27 due to surface effects, NH₂-MIL-53(Al) nanoparticles having an average particle size of 50 nm
28 (Fig. S13) were synthesized according to the recipe reported by Wu *et al.*⁶⁵ MMMs with 10 wt%
29 loading of NH₂-MIL-53(Al) nanoparticles were prepared and treated at 350 °C. Gas separation
30 results showed that the MMMs incorporated with NH₂-MIL-53(Al) nanoparticles did not show
31 improvements in CO₂/CH₄ selectivity. In contrast, CO₂/CH₄ selectivity decreased and CO₂
32 permeability increased (Table S2). It is likely that the smaller particles tend to agglomerate and
33 create interfacial gaps/voids when dispersed into the polymer matrix, resulting in non-selective
34 gas transport pathways, despite efforts to better disperse the non-dried NH₂-MIL-53(Al)
35 nanoparticles via sonication prior to MMM preparation. SEM imaging of the NH₂-MIL-53(Al)
36
37
38
39
40
41
42
43
44
45
46
47
48
49
50
51
52
53
54
55
56
57
58
59
60

nanoparticle loaded MMM cross-section is shown in Fig. S14. Agglomerations and interfacial gaps are observed throughout the MMM. These results suggest that the particle size of the fillers does play a crucial role in its dispersion in the polymer. Large agglomeration of the particles within the polymer interact poorly with the polymer, resulting in non-selective defects. Similar issue has also been encountered and reported for MMM loaded with nanosized MOF-74,⁶⁶ ZIF-8⁶⁷ and NH₂-MIL-53.⁶⁸ For example, the preparation of MMMs based on polybenzimidazole (PBI) and ZIF-8 nanoparticles of different average sizes (50, 70 and 150 nm) has been documented.⁶⁷ According to the gas separation results, both permeability and selectivity of the MMMs were dramatically reduced as the filler size decreased, due to the higher degree of nanoparticle agglomeration owing to their higher external surface area. Similarly, particles agglomeration has also been reported on the top layer of MMMs prepared from 100 nm-sized NH₂-MIL 53(Al) filler even at low filler loading (10 wt%).⁶⁸ Therefore, in some cases (depending on MOF type), agglomeration of MOF filler in the polymer matrix could not be avoided despite nanosized MOF fillers are used for the fabrication of MOF-based MMMs.

The pore dimensions of NH₂-MIL-53(Al) (7.5 Å) are far larger than the kinetic diameters of CO₂ (3.3 Å) and CH₄ (3.8 Å),³¹ which is contradicting the outstanding selectivities achieved for the highly loaded MMMs.³⁶ The selectivity increase thus has to be fully ascribed to the partial blockage of the pore mouths by the penetrated polymer chains and the densified matrix around it.^{36,58} NH₂-MIL-53 crystals were reported to transform to two main possible conformations that can be distinguished: the *lp* and *np* forms when activated at different temperature,⁵² which is in full agreement with our XRD data as presented in Figure 1D. Accordingly to our results (Figure 1D), *lp* form is obtained when the NH₂-MIL-53(Al) loaded MMMs were treated at 250 and 350 °C, whereas the *np* form is obtained when the NH₂-MIL-53(Al) loaded MMMs were treated at 100

1
2
3 and 160 °C. From the gas separation point of view, gas transport would have been enhanced with
4
5 NH₂-MIL-53(Al) in its *lp* form in the MMM but the selectivity would have decreased. While in its
6
7 *np* form NH₂-MIL-53(Al) would serve as a selective molecular sieve to give high CO₂/CH₄
8
9 selectivity. At the same time CO₂ permeability would decrease. In this work, we demonstrate that
10
11 the penetration of the polymer chains into the pores of NH₂-MIL-53(Al) could maintain its *lp*
12
13 configuration. Coupled with the simultaneous polymer-polymer crosslinking in the bulk of the
14
15 membrane, a network that is sufficiently dense to hinder the permeation of CH₄ is thus formed as
16
17 illustrated by the very limited sacrifices in CO₂ permeability that accompany this exceptional
18
19 improvement in selectivity, contrasting earlier work with comparable systems.³⁷ This very modest
20
21 reduction in CO₂ permeability is possible thanks to the fact that only MOF pore entrances were
22
23 crosslinked by the polymer chains, thus retaining the *lp* form.
24
25
26
27
28

29
30 A major drawback for membrane-based gas separations is the loss in selectivity that is
31
32 often encountered as a result of excessive polymer mobility due to interaction with CO₂ at high
33
34 feed pressure. The crosslinked MMM with 40 wt% MOF loading was therefore evaluated for its
35
36 plasticization resistance at high feed pressure (40 bar). The gas separation measurement performed
37
38 at 40 bar confirmed that the crosslinked MMM could retain its high CO₂/CH₄ selectivity (Table
39
40 S3). It is also important to mention that early research in this field has reported about the issue of
41
42 embrittlement in MOF-loaded MMMs when MOF loading increases.⁶⁹ The MMMs will become
43
44 brittle when the filler loading increases to > 30 wt%. At a very high filler loadings (60 wt%), the
45
46 MMMs were not selective for CO₂/CH₄ separation.⁷⁰ However, according to the measured
47
48 mechanical properties of our MMMs treated at different temperatures (100-350 °C), the tensile
49
50 strength of the MMMs with 40 wt% loading increases from 24.5 to 32.7 MPa with increasing
51
52 temperature from 100 to 350 °C as shown in Table S1 and Figure S5 which can be explained from
53
54
55
56
57
58
59
60

1
2
3 the observed membrane densification as a result of crosslinking. Although the MMMs with 40
4 wt% loading showed a sign of brittleness in comparison to the unfilled polyimide membranes, the
5
6 fabricated MMMs with 40 wt% MOF loading and thermally treated at 350 °C could still survive
7
8 at pressure up to 10 bar and gave promising CO₂/CH₄ selectivity (Figure 4D).
9

10
11
12 The position of a polymer's gas permeability data relative to the Roberson upper bound is
13 used as the universal performance indicator for assessing its potential for the separation of CO₂
14 from CH₄, as depicted in Figure 3E.⁹ Figure 3E and Table S2 show the CO₂/CH₄ selectivities and
15 CO₂ permeabilities for the presented MMMs compared to other NH₂-MIL-53(Al) loaded MMMs
16 obtained from literature. The MMM treated at 350 °C with 40 wt% loading achieved the highest
17 mixed-gas CO₂/CH₄ selectivity of 153 with a CO₂ permeability of 5.8 Barrer (purple circles), and
18 hit the 2008 upper-bound, clearly outperforming the unfilled Matrimid® membranes (blue
19 diamonds) and earlier reported NH₂-MIL-53(Al) loaded MMMs (orange squares). These
20 crosslinked MMMs also reached the state-of-the-art separation performances of MMMs based on
21 commercially available polymers embedding other MOF-types (Table S3).¹⁹
22
23
24
25
26
27
28
29
30
31
32
33
34
35

36 **Conclusions**

37
38
39 In summary, NH₂-MIL-53(Al) loaded MMMs with excellent MOF dispersion and polymer-MOF
40 adhesion were prepared. As a result of thermal treatment at 350 °C, the physiochemical properties
41 e.g. solubility, density, glass transition temperature and mechanical strength of the thermally
42 treated MMMs were enhanced. Treatment of the MMMs at high temperatures induced thermo-
43 oxidative crosslinking of the PI matrix, as well as the covalent bonding between the polymer and
44 the NH₂ groups at the MOF pore mouth. During the thermal treatment, the MOF underwent a
45 configurational transition from its *np* to *lp* form, which allowed the polymer chains to partially
46 penetrate and crosslink to the amine groups at the entrance of the MOF pores. The anchoring of
47
48
49
50
51
52
53
54
55
56
57
58
59
60

1
2
3 the PI-chains forced the MOF to retain its *lp* form. As a result, very high mixed gas CO₂/CH₄
4
5 selectivities were thus realized without sacrificing too much permeability. These crosslinked
6
7 MMMs show exciting potential for purification of biogas and natural gas, but also for use in liquid
8
9 and other gas phase separations.
10

11 12 13 ASSOCIATED CONTENT

14 15 16 **Supporting Information.**

17
18
19
20 Supplemental Information includes characterization of MOF, PI and mixed-matrix membranes
21
22 by SEM (Figures S1, S10, S13, S14), TGA (Figure S2), solubility test (Figure S3), ATR-FTIR
23
24 (Figure S4), tensile strength (Figure S5 and Table S1)), XRD (Figures S6-S9), TEM (Figure
25
26 S11), CO₂ adsorption isotherms (Figure S12) and gas separation results (Tables S2-3).
27
28
29

30 The following files are available free of charge.

31
32 Supporting Information (PDF)
33
34
35
36
37

38 39 40 AUTHOR INFORMATION

41 42 **Corresponding Author**

43
44 * E-mail: likhong.wee@kuleuven.be; ivo.vankelecom@kuleuven.be
45
46

47 48 **Present Addresses**

49
50 †Adsorption & Advanced Materials, Department of Chemical Engineering and Biotechnology,
51
52 University of Cambridge, West Cambridge Site, Philippa Fawcett Drive, Cambridge, CB3 0AS,
53
54 United Kingdom
55
56
57
58
59
60

Author Contributions

A.K. executed the experiments including material synthesis, membrane fabrication, characterization and gas separation evaluation. L.H.W. directed the membrane characterization and analyzed all the data. K.S. acquired and analyzed the TEM results in the supervision of S.B. A.K. wrote the first draft of the manuscript and completed by L.H.W. with input from all authors. I.F.J.V. initiated the project and obtained the funding. L.H.W. and I.F.J.V. supervised the project.

Notes

The authors declare no competing financial interest.

ACKNOWLEDGMENT

A.K. is grateful to the Erasmus Mundus Doctorate in Membrane Engineering (EUDIME) programme. L.H.W. thanks the FWO-Vlaanderen for a postdoctoral research fellowships under contract number 12M1418N. The authors would like to thank Methusalem and IAP-PAI for research funding. S.B. acknowledges financial support from European Research Council (ERC) (ERC Starting Grant No. 335078-COLOURATOM). We are also grateful to Frank Mathijs (KU Leuven) for the mechanical tests, Bart Goderis and Olivier Verkinderen for the DSC measurements and Huntsman (Switzerland) for providing the Matrimid® polymer.

REFERENCES

1. Baker, R.W.; Lokhandwala, K. Natural Gas Processing with Membranes: An Overview. *Ind. Eng. Chem. Res.* **2008**, *47*, 2109–2121.
2. Baker, R. W. *Membrane Technology and Applications*, John Wiley & Sons Ltd., Chichester, UK, 2012; pp. 1–14.

- 1
2
3 3. Tanaka, K.; Okamoto, K. -I. *Materials Science of Membranes for Gas and Vapor*
4
5 *Separation*, Yampolskii, Y., Pinnau, I., Freeman B., Eds., John Wiley & Sons Ltd, Chichester,
6
7 UK, 2006; pp. 271–291.
8
9
- 10
11 4. Bachman, J. E.; Long, J. R. Plasticization-resistant Ni₂(dobdc)/polyimide Composite
12
13 Membranes for the Removal of CO₂ from Natural Gas. *Energy Environ. Sci.* **2016**, *9*, 2031–2036.
14
15
- 16
17 5. Thornton, A. W.; Dubbeldam, D.; Liu, M. S.; Ladewig, B. P.; Hill, A. J.; Hill, M. R.
18
19 Feasibility of Zeolitic Imidazolate Framework Membranes for Clean Energy Applications. *Energy*
20
21 *Environ. Sci.* **2012**, *5*, 7637–7646.
22
23
- 24
25 6. Makaruk, A.; Miltner, M.; Harasek, M. Membrane Biogas Upgrading Processes for the
26
27 Production of Natural Gas Substitute. *Sep. Purif. Technol.* **2010**, *74*, 83–92.
28
29
- 30
31 7. Scholz, M.; Melin, T.; Wessling, M. Transforming Biogas into Biomethane using
32
33 Membrane Technology. *Renew. Sustain. Energy Rev.* **2013**, *17*, 199–212.
34
35
- 36
37 8. Robeson, L. M. Correlation of Separation Factor versus Permeability for Polymeric
38
39 Membranes. *J. Membr. Sci.* **1991**, *62*, 165–185.
40
- 41
42 9. Robeson, L. M. The Upper Bound Revisited. *J. Membr. Sci.* **2008**, *320*, 390–400.
43
44
- 45
46 10. Hillock, A. M. W.; Miller, S. J.; Koros, W. J. Crosslinked Mixed Matrix Membranes for
47
48 the Purification of Natural Gas: Effects of Sieve Surface Modification. *J. Membr. Sci.* **2008**, *314*,
49
50 193–199.
51
- 52
53 11. Wind, J. D.; Paul, D. R.; Koros, W. J. Natural Gas Permeation in Polyimide Membranes.
54
55 *J. Membr. Sci.* **2004**, *228*, 227–236.
56
57
58
59
60

- 1
2
3 12. Cao, C.; Chung, T. -S.; Liu, Y.; Wang, R.; Pramod, K. P. Chemical Cross-linking
4 Modification of 6FDA-2, 6-DAT Hollow Fiber Membranes for Natural Gas Separation J. Membr.
5
6 Sci. **2003**, *216*, 257–268.
7
8
9
10
11 13. Chung, T. -S.; Jiang, L.; Li, Y.; Kulprathipanja, S. Mixed Matrix Membranes (MMMs)
12 Comprising Organic Polymers with Dispersed Inorganic Fillers for Gas Separation. Prog. Polym.
13
14 Sci. **2007**, *32*, 483–507.
15
16
17
18
19 14. Mahajan, R.; Koros, W. J. Factors Controlling Successful Formation of Mixed-matrix Gas
20 Separation Materials. Ind. Eng. Chem. Res. **2000**, *39*, 2692–2696.
21
22
23
24
25 15. Sudhir, S. K.; David J. H.; David R. C. Aspi N. P. Gas Separation Membrane with
26 Organosilicon-treated Molecular Sieve. U.S. Patent 6508860B1, January 21, 2003.
27
28
29
30
31 16. Guiver, M. D.; Thi, H. N. L.; Robertson, G. P. *Composite Gas Separation Membranes*.
32 U.S. Patent 6605140. August 12, 2003.
33
34
35
36 17. Wang, S.; Wu, Y.; Zhang, N.; He, G.; Xin, Q.; Wu, X.; Wu, H.; Cao, X.; Guiver, M. D.;
37 Jiang, Z. A Highly Permeable Graphene Oxide Membrane with Fast and Selective Transport
38 Nanochannels for Efficient Carbon Capture. Energy Environ. Sci. **2016**, *9*, 3107–3112.
39
40
41
42
43 18. Jiang, X.; Li, S.; He, S.; Bai, Y.; Shao, L. Interface Manipulation of CO₂-philic Composite
44 Membranes Containing Designed UiO-66 Derivatives Towards Highly Efficient CO₂ Capture. J.
45 Mater. Chem. A **2018**, *6*, 15064–15073.
46
47
48
49
50
51
52
53
54
55
56
57
58
59
60

- 1
2
3 19. Jiang, X.; Li, S.; Bai, Y.; Shao, L. Ultra-facile Aqueous Synthesis of Nanoporous Zeolitic
4 Imidazolate Framework Membranes for Hydrogen Purification and Olefin/Paraffin Separation. *J.*
5
6
7
8 *Mater. Chem. A* **2019**, *7*, 10898–10904.
9
- 10
11 20. Li, J. -R.; Kuppler, R. J.; Zhou, H. -C. Selective Gas Adsorption and Separation in Metal–
12
13
14
15
16
17
18
19
20
21
22
23
24
25
26
27
28
29
30
31
32
33
34
35
36
37
38
39
40
41
42
43
44
45
46
47
48
49
50
51
52
53
54
55
56
57
58
59
60
20. Li, J. -R.; Kuppler, R. J.; Zhou, H. -C. Selective Gas Adsorption and Separation in Metal–
organic Frameworks. *Chem. Soc. Rev.* **2009**, *38*, 1477–1504.
21. Seoane, B.; Coronas, J.; Gascon, I.; Benavides, M. E.; Karvan, O.; Caro, J.; Kapteijn, F.;
Gascon, J. Metal–organic Framework Based Mixed Matrix Membranes: A Solution for Highly
Efficient CO₂ Capture? *Chem. Soc. Rev.* **2015**, *44*, 2421–2454.
22. Férey, G. Hybrid Porous Solids: Past, Present, Future. *Chem. Soc. Rev.* **2008**, *37*, 191–214.
23. Férey, G.; Serre, C. Large Breathing Effects in Three-dimensional Porous Hybrid Matter:
Facts, Analyses, Rules and Consequences. *Chem. Soc. Rev.* **2009**, *38*, 1380–1399.
24. Alhamami, M.; Doan, H.; Cheng, C. -H. A Review on Breathing Behaviors of Metal-
organic-Frameworks (MOFs) for Gas Adsorption. *Materials* **2014**, *7*, 3198–3250.
25. Stavitski, E.; Pidko, E. A.; Couck, S.; Remy, T.; Hensen, E. J. M.; Weckhuysen, B. M.;
Denayer, J.; Gascon, J.; Kapteijn, F. Complexity Behind CO₂ Capture on NH₂-MIL-53(Al).
Langmuir **2011**, *27*, 3970–3976.
26. Liu, Y.; Her, J. -H.; Dailly, A.; Ramirez-Cuesta, A. J.; Neumann, D. A.; Brown, C. M.
Reversible Structural Transition in MIL-53 with Large Temperature Hysteresis. *J. Am. Chem. Soc.*
2008, *130*, 11813–11818.

- 1
2
3 27. Salles, F.; Ghoufi, A.; Maurin, G.; Bell, R. G.; Mellot-Draznieks, C.; Férey, G. Molecular
4 Dynamics Simulations of Breathing MOFs: Structural Transformations of MIL-53(Cr) upon
5 Thermal Activation and CO₂ Adsorption. *Angew. Chem. Int. Ed.* **2008**, *120*, 8487–8491.
6
7
8
9
10
11 28. Trung, T. K.; Trens, P.; Tanchoux, N.; Bourrelly, S.; Llewellyn, P. L.; Loera-Serna, S.;
12 Serre, C.; Loiseau, T.; Fajula, F.; Férey, G. Hydrocarbon Adsorption in the Flexible Metal Organic
13 Frameworks MIL-53(Al, Cr). *J. Am. Chem. Soc.* **2008**, *130*, 16926–16932.
14
15
16
17
18
19 29. Llewellyn, P. L.; Bourrelly, S.; Serre, C.; Filinchuk, Y.; Férey, G. How Hydration
20 Drastically Improves Adsorption Selectivity for CO₂ over CH₄ in the Flexible Chromium
21 Terephthalate MIL-53. *Angew. Chem. Int. Ed.* **2006**, *45*, 7751–7754.
22
23
24
25
26
27 30. Zhang, F.; Zou, X.; Gao, X.; Fan, S.; Sun, F.; Ren, H.; Zhu, G. Hydrogen Selective NH₂-
28 MIL-53(Al) MOF Membranes with High Permeability. *Adv. Funct. Mater.* **2012**, *22*, 3583–3590.
29
30
31
32
33 31. Couck, S.; Rémy, T.; Baron, G. V.; Gascon, J.; Kapteijn, F.; Denayer, J. F. M. A Pulse
34 Chromatographic Study of the Adsorption Properties of the Amino-MIL-53 (Al) Metal–organic
35 Framework. *Phys. Chem. Chem. Phys.* **2010**, *12*, 9413–9418.
36
37
38
39
40
41 32. Boutin, A.; Couck, S.; Coudert, F. X.; Serra-Crespo, P.; Gascon, J.; Kapteijn, F.; Fuchs,
42 A.H.; Denayer, J. F. M. Thermodynamic Analysis of the Breathing of Amino-functionalized MIL-
43 53(Al) upon CO₂ Adsorption. *Micropor. Mesopor. Mater.* **2011**, *140*, 108–113.
44
45
46
47
48
49 33. Rodenas, T.; Luz, I.; Prieto, G.; Seoane, B.; Miro, H.; Corma, A.; Kapteijn, F.; Llabrés i
50 Xamena, F. X.; Gascon, J. Metal-organic Framework Nanosheets in Polymer Composite Materials
51 for Gas Separation. *Nat. Mater.* **2015**, *14*, 48–55.
52
53
54
55
56
57
58
59
60

- 1
2
3 34. Song, Q.; Nataraj, S. K.; Roussenova, M. V.; Tan, J. C.; Hughes, D. J.; Li, W.; Bourgoïn,
4 P.; Alam, M. A.; Cheetham, A. K.; Al-Muhtaseb, S. A.; Sivaniah, E. Zeolitic Imidazolate
5 Framework (ZIF-8) Based Polymer Nanocomposite Membranes for Gas Separation. *Energy*
6 *Environ. Sci.* **2012**, *5*, 8359–8369.
7
8
9
10
11
12
13 35. Sabetghadam, A.; Seoane, B.; Keskin, D.; Duim, N.; Rodenas, T.; Shahid, S.; Sorribas, S.;
14 Le Guillouzer, C.; Clet, G.; Tellez, C.; Daturi, M.; Coronas, J.; Kapteijn, F.; Gascon, J. Metal
15 Organic Framework Crystals in Mixed-matrix Membranes: Impact of the Filler Morphology on
16 the Gas Separation Performance. *Adv. Funct. Mater.* **2016**, *26*, 3154–3163.
17
18
19
20
21
22
23 36. Rodenas, T., van Dalen, M., García-Pérez, E., Serra-Crespo, P., Zornoza, B., Kapteijn, F.,
24 and Gascon, J. (2014). Visualizing MOF Mixed Matrix Membranes at the Nanoscale: Towards
25 Structure-performance Relationships in CO₂/CH₄ Separation over NH₂-MIL-53(Al)@PI. *Adv.*
26 *Funct. Mater.* *24*, 249–256.
27
28
29
30
31
32
33 37. Kertik, A.; Wee, L. H.; Pffannmüller, M.; Bals, S.; Martens, J. A.; Vankelecom, I. F. J.
34 Highly Selective Gas Separation Membrane using In Situ Amorphised Metal–organic
35 Frameworks. *Energy Environ. Sci.* **2017**, *10*, 2342–2351.
36
37
38
39
40
41
42 38. Khan, A. L.; Basu, S.; Cano-Odena, A.; Vankelecom, I. F. J. Novel High Throughput
43 Equipment for Membrane-based Gas Separations. *J. Membr. Sci.* **2010**, *354*, 32–39.
44
45
46
47 39. Song, Q.; Cao, S.; Pritchard, R. H.; Ghalei, B.; Al-Muhtaseb, S. A.; Terentjev, E. M.;
48 Cheetham, A. K.; Sivaniah, E. Controlled Thermal Oxidative Crosslinking of Polymers of Intrinsic
49 Microporosity Towards Tunable Molecular Sieve Membranes. *Nat. Commun.* **2014**, *5*, 4813.
50
51
52
53
54
55
56
57
58
59
60

- 1
2
3 40. Martínez-Izquierdo, L.; Malankowska, M.; Sánchez-Láinez, J.; Téllez, C.; Coronas, J.
4
5 Poly(ether-block-amide) Copolymer Membrane for CO₂/N₂ Separation: The Influence of the
6
7 Casting Solution Concentration on Its Morphology, Thermal Properties and Gas Separation
8
9 Performance. *R. Soc. open sci.* **2019**, *6*, 190866.
- 10
11
12
13 41. Kuroda, S.; Mita, I. Degradation of Aromatic Polymers—II. The Crosslinking during
14
15 Thermal and Thermo-oxidative Degradation of a Polyimide. *Eur. Polym. J.* **1989**, *25*, 611–620.
- 16
17
18
19 42. Anjum, M. W.; Vermoortele, F.; Khan, A. L.; Bueken, B.; De Vos, D. E.; Vankelecom, F.
20
21 J. Modulated UiO-66-Based Mixed-Matrix Membranes for CO₂ Separation. *ACS Appl. Mater.*
22
23 *Interfaces* **2015**, *7*, 25193–25201.
- 24
25
26
27 43. Tin, P. S.; Chung, T. S.; Liu, Y.; Wang, R.; Liu, S. L.; Pramoda, K. P. Effects of Cross-
28
29 linking Modification on Gas Separation Performance of Matrimid Membranes. *J. Membr. Sci.*
30
31 **2003**, *225*, 77–90.
- 32
33
34
35 44. Toh, Y. H. S.; Lim, F. W.; Livingston, A. G. Polymeric Membranes for Nanofiltration in
36
37 Polar Aprotic Solvents. *J. Membr. Sci.* **2007**, *301*, 3–10.
- 38
39
40
41 45. Nielsen, L. E. Cross-linking Effect on Physical Properties of Polymers. *J. Macromol. Sci.*
42
43 *Part C Polym. Rev.* **1969**, *3*, 69–103.
- 44
45
46
47 46. Schneemann, A.; Bon, V.; Schwedler, I.; Senkovska, I.; Kaskel, S.; Fischer, R. A. Flexible
48
49 Metal–organic Frameworks. *Chem. Soc. Rev.* **2014**, *43*, 6062–6096.
- 50
51
52
53 47. Llewellyn, P. L.; Bourrelly, S.; Serre, C.; Filinchuk, Y.; Férey, G. How Hydration
54
55 Drastically Improves Adsorption Selectivity for CO₂ over CH₄ in the Flexible Chromium
56
57 Terephthalate MIL-53. *Angew. Chem. Int. Ed.* **2006**, *45*, 7751–7754.
- 58
59
60

- 1
2
3 48. Goesten, M. G.; Gupta, K. B. S. S.; Ramos-Fernandez, E. V.; Khajavi, H.; Gascon, J.;
4 Kapteijn, F. Chloromethylation as a Functionalisation Pathway for Metal–organic Frameworks.
5
6 *CrystEngComm* **2012**, *14*, 4109–4111.
7
8
9
10
11 49. Cheng, X.; Zhang, A.; Hou, K.; Liu, M.; Wang, Y.; Song, C.; Zhang, G.; Guo, X. Size- and
12
13 Morphology-controlled NH₂-MIL-53(Al) Prepared in DMF–water Mixed Solvents. *Dalton Trans.*
14
15 **2013**, *42*, 13698–13705.
16
17
18
19 50. Serra-Crespo, P.; Gobechiya, E.; Ramos-Fernandez, E. V.; Juan-Alcañiz, J.; Martinez-
20
21 Joaristi, A.; Stavitski, E.; Kirschhock, C. E. A.; Martens, J. A.; Kapteijn, F.; Gascon, J. Interplay
22
23 of Metal Node and Amine Functionality in NH₂-MIL-53: Modulating Breathing Behavior through
24
25 Intra-framework Interactions. *Langmuir* **2012**, *28*, 12916–12922.
26
27
28
29 51. Seoane, B.; Téllez, C.; Coronas, J.; Staudt, C. NH₂-MIL-53(Al) and NH₂-MIL-101(Al) in
30
31 Sulfur-containing Copolyimide Mixed Matrix Membranes for Gas Separation. *Sep. Purif. Technol.*
32
33 **2013**, *111*, 72–81.
34
35
36
37 52. Hsieh, J. O.; Balkus Jr. K. J.; Ferraris, J. P.; Musselman, I. H. MIL-53 Frameworks in
38
39 Mixed-matrix Membranes. *Micropor. Mesopor. Mater.* **2014**, *196*, 1651–74.
40
41
42
43 53. Zhang, Y.; Balkus Jr. K. J.; Musselman, I. H.; Ferraris, J. P. Mixed-matrix Membranes
44
45 Composed of Matrimid® and Mesoporous ZSM-5 Nanoparticles. *J. Membr. Sci.* **2008**, *325*, 28–39.
46
47
48
49 54. Duan, P.; Moreton, J. C.; Tavares, S. R.; Semino, R.; Guillaume Maurin, G.; Cohen, S. M.;
50
51 Schmidt-Rohr, K. Polymer Infiltration into Metal–Organic Frameworks in Mixed-Matrix
52
53 Membranes Detected in Situ by NMR. *J. Am. Chem. Soc.* **2019**, *141*, 7589–7595.
54
55
56
57
58
59
60

- 1
2
3 55. Semino, R.; Moreton, J. C.; Ramsahye, N. A.; Cohen, S. M.; Maurin, G. Understanding
4 the Origins of Metal–organic Framework/Polymer Compatibility. *Chem. Sci.* **2018**, *9*, 315–324.
5
6
7
8
9 56. Mahajan, R.; Burns, R.; Schaeffer, M.; Koros, W. J. Challenges in Forming Successful
10 Mixed Matrix Membranes with Rigid Polymeric Materials. *J. Appl. Polym. Sci.* **2002**, *86*,
11 881–890.
12
13
14
15
16
17 57. Li, Y.; Chung, T. S.; Cao, C.; Kulprathipanja, S. The Effects of Polymer Chain
18 Rigidification, Zeolite Pore Size and Pore Blockage on Polyethersulfone (PES)-zeolite A Mixed
19 Matrix Membranes. *J. Membr. Sci.* **2005**, *260*, 45–55.
20
21
22
23
24
25 58. Dong, G., Li, H.; Chen, V. Challenges and Opportunities for Mixed-matrix Membranes for
26 Gas Separation. *J. Mater. Chem. A* **2013**, *1*, 4610–4630.
27
28
29
30
31 59. Loiseau, T.; Serre, C.; Huguenard, C.; Fink, G.; Taulelle, F.; Henry, M.; Bataille, T.; Férey,
32 G. A Rationale for the Large Breathing of the Porous Aluminum Terephthalate (MIL-53) upon
33 Hydration. *Chem. Eur. J.* **2004**, *10*, 1373–1382.
34
35
36
37
38 60. Rodenas, T.; van Dalen, M.; Serra-Crespo, P.; Kapteijn, F.; Gascon, J. Mixed Matrix
39 Membranes Based on NH₂-functionalized MIL-type MOFs: Influence of Structural and
40 Operational Parameters on the CO₂/CH₄ Separation Performance. *Micropor. Mesopor. Mater.*
41 **2014**, *192*, 35–42.
42
43
44
45
46
47
48 61. Feijani, E. A.; Mahdavi, H.; Tavasoli, A. Poly(vinylidene fluoride) Based Mixed Matrix
49 Membranes Comprising Metal Organic Frameworks for Gas Separation Applications. *Chem. Eng.*
50 *Res. Des.* **2015**, *96*, 87–102.
51
52
53
54
55
56
57
58
59
60

- 1
2
3 62. Chen, X. Y.; Hoang, V. -T.; Rodrigue, D.; Kaliaguine, S. Optimization of Continuous
4 Phase in Amino-functionalized Metal–organic Framework (MIL-53) Based Co-polyimide Mixed
5 Matrix Membranes for CO₂/CH₄ Separation. *RSC Adv.* **2013**, *3*, 24266–24279.
6
7
8
9
10
11 63. Zornoza, B.; Martinez-Joaristi, A.; Serra-Crespo, O.; Tellez, C.; Coronas, J.; Gascon, J.;
12 Kapteijn, F. Functionalized Flexible MOFs as Fillers in Mixed Matrix Membranes for Highly
13 Selective Separation of CO₂ from CH₄ at Elevated Pressures. *Chem. Commun.* **2011**, *47*,
14 9522–9524.
15
16
17
18
19
20
21 64. Zhang, Y.; Feng, X.; Yuan, S.; Zhou, J.; Wang, B. Challenges and Recent Advances in
22 MOF–polymer Composite Membranes for Gas Separation. *Inorg. Chem. Front.* **2016**, *3*, 896–909.
23
24
25
26
27 65. Wu, G.; Jiang, M.; Zhang, T.; Jia, Z. Tunable Pervaporation Performance of Modified
28 MIL-53(Al)-NH₂/poly(vinyl alcohol) Mixed Matrix Membranes. *J. Membr. Sci.* **2016**, *507*, 72–80.
29
30
31
32 66. Bachman, J. E.; Smith, Z. P.; Li, T.; Xu, T.; Long, J. R. Enhanced Ethylene Separation
33 and Plasticization Resistance in Polymer Membranes Incorporating Metal–organic Framework
34 Nanocrystals. *Nat. Mater.* **2016**, *15*, 845–849.
35
36
37
38
39
40 67. Sánchez-Laínez, J.; Zornoza, B.; Friebe, S.; Caro, J.; Cao, S.; Sabetghadam, A.; Seoane,
41 B.; Gascon, J.; Kapteijn, F.; Guillouzer, C. L.; Clet, G.; Daturi, M.; Téllez, C.; Coronas, J.
42 Influence of ZIF-8 Particle Size in the Performance of Polybenzimidazole Mixed Matrix
43 Membranes for Pre-combustion CO₂ Capture and Its Validation Through Interlaboratory Test. *J.*
44 *Membr. Sci.* **2016**, *515*, 45–53.
45
46
47
48
49
50
51
52
53 68. Abedini, R.; Omidkhah, M.; Dorosti, F. Highly Permeable Poly(4-methyl-1-pentyne)/NH₂-
54 MIL 53 (Al) Mixed Matrix Membrane for CO₂/CH₄ Separation. *RSC Adv.* **2014**, *4*, 36522–36537.
55
56
57
58
59
60

1
2
3 69. Smith, Z. P.; Bachman, H. E.; Li, T.; Gludovatz, B.; Kusuma, V. A.; Xu, T.; Hopkinson,
4 D. P.; Ritchie, R. O.; Long, J. R. Increasing M₂(dobdc) Loading in Selective Mixed-Matrix
5 Membranes: A Rubber Toughening Approach. *Chem. Mater.* **2018**, *30*, 1484–1495.
6
7

8
9
10
11 70. Ordoñez, M. J. C.; Balkus Jr. K. J.; Ferraris, J. P.; Musselman, I. H. Molecular sieving
12 Realized with ZIF-8/Matrimid[®] Mixed-matrix Membranes. *J. Membr. Sci.* **2010**, *361*, 28–37.
13
14
15
16
17
18
19
20
21
22
23
24
25
26
27
28
29
30
31
32
33
34
35
36
37
38
39
40
41
42
43
44
45
46
47
48
49
50
51
52

53 TOC
54
55
56
57
58
59
60

